α-nucleus scattering in angular momentum space

I. Jamir, E. F. P. Lyngdoh, and C. S. Shastry
Department of Physics, North Eastern Hill University, Shillong 793 022, India
(Received 30 June 1997; revised manuscript received 10 September 1997)

We provide an interpretation of anomalous large angle scattering (ALAS) for α-nucleus systems by decomposing the full scattering amplitude $A(\theta)$ into three components in l space viz. $A_I(\theta)$, $A_S(\theta)$, and $A_O(\theta)$ corresponding to interior, surface, and predominantly Coulombic outer partial waves and show that it is the interference between $A_S(\theta)$ and $A_O(\theta)$ terms which is primarily responsible for ALAS. The interpretation of ALAS given here is complementary to that of Brink and Takigawa where the nuclear S matrix was split into a barrier region part and an interior region part in coordinate space. We also compute the resonance-like poles of the S matrix in the complex energy plane and find that one can associate broad barrier region resonance poles with the few partial waves which contribute to $A_S(\theta)$. [S0556-2813(98)00101-0]

PACS number(s): 24.10.Ht, 25.55.Ci, 25.70.−z

Anomalous large angle scattering (ALAS) has been studied by several workers using different approaches. Within the framework of phenomenological approaches, potentials have been constructed which can reproduce the ALAS data in α-nucleus systems [1–6] as well as in nucleus-nucleus systems such as $^{16}O+^{28}Si$ [7–9]. Nuclear potentials with the form factor $f(r)=\{1+\exp[(r-R)/\nu a]\}^{-\nu}$ used by Gubler *et al.* [4] and Delbar *et al.* [2] show that simple potentials can give rise to ALAS. ALAS potentials can also be constructed using microscopic approaches like the double-folding model [10]. Frahn *et al.* [11–13] have used phenomenological closed form expressions for the S matrix to analyze nuclear scattering problems including ALAS. Brink and Takigawa [14] have explained ALAS in terms of the interference of internal and barrier waves, whereas Shastry and Parija [15] and Parija *et al.* [16] have used the concept of interference of the surface region and outer region amplitudes. In this paper, we undertake a detailed analysis of the phenomenological optical potential approaches for α-nucleus scattering and the corresponding features of the S matrix and their correlation with the back angle oscillations.

The potential used by Gubler *et al.* [4] to reproduce ALAS in the $\alpha+^{40}Ca$ system has the form

$$V(r)=-V_0\left[1+\exp\left(\frac{r-R_R}{\nu a_R}\right)\right]^{-\nu}-iW_0\left[1+\exp\left(\frac{r-R_I}{a_I}\right)\right]^{-1}+V_C(r). \tag{1.1}$$

Here, $R_R=r_R A_2^{1/3}$ and $R_I=r_I A_2^{1/3}$ pertain to the target nucleus, $V_C(r)$ is the Coulomb potential for a uniformly charged sphere of radius R_C, and ν is the parameter which plays a crucial role in fitting the experimental data. Gubler *et al.* have fitted the data with $\nu=5$ at $E_{\rm lab}=29$ MeV for which the grazing partial wave is $l_g\simeq 13$. We have also studied the potential at this energy for various values of ν. Defining $V_{\rm eff}(r)=V(r)+V_l(r)$, where $V_l(r)$ is the centrifugal term, we find that whereas for $\nu<5$, the potential shows a distinct pocket, it is monotonic for $\nu>5$ and at $\nu=5$, it shows maximum flatness around the barrier region. This means that the parameter $\nu=5$ generates an effective potential which can give rise to surface waves or orbiting-like phenomenon. Also, the imaginary part of $V_{\rm eff}(r)$ becomes very small for $r>6$ fm leaving a substantial part of the effective potential practically surface transparent. We have verified that a similar feature is present in other phenomenological α-nucleus potentials such as those of Michel *et al.* [5] for $\alpha+^{16}O$ and Lega and Macq [6] for $\alpha+^{26}Mg$. Thus in the surface region, the potentials which reproduce back angle oscillations have (i) slow variation of the effective potential around $l=l_g$ and (ii) the imaginary part is quite small.

We also observe that the α-nucleus potentials have three turning points for only a few partial waves. A typical case is shown in Fig. 1 for the $\alpha+^{40}Ca$ system at $E_{\rm lab}=29$ MeV. Due to the flatness of the effective potential, the separation between the two outer turning points is quite large. Thus for these partial waves, a rather wide barrier is to be traversed to tunnel into the pocket region and for smaller partial waves for which the height of the barrier is less than the center-of-

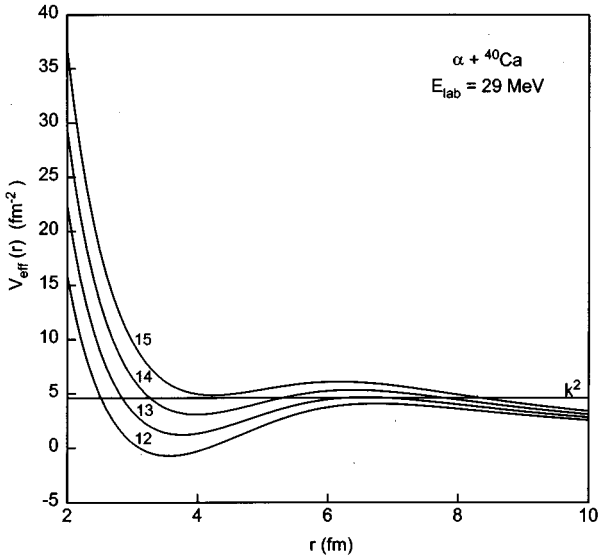

FIG. 1. Plot of $\mathrm{Re}V_{\rm eff}(r)$ defined by Eq. (1.1) for partial waves around l_g. The line marked k^2 corresponds to the incident energy. $l=13$ and 14 have three turning points. The potential parameters [4] are $V_0=232.5$ MeV, $r_R=1.89$ fm, $a_R=0.37$ fm, $W_0=35.15$ MeV, $r_I=0.74$ fm, $a_I=1.01$ fm, $r_C=1.3$ fm.

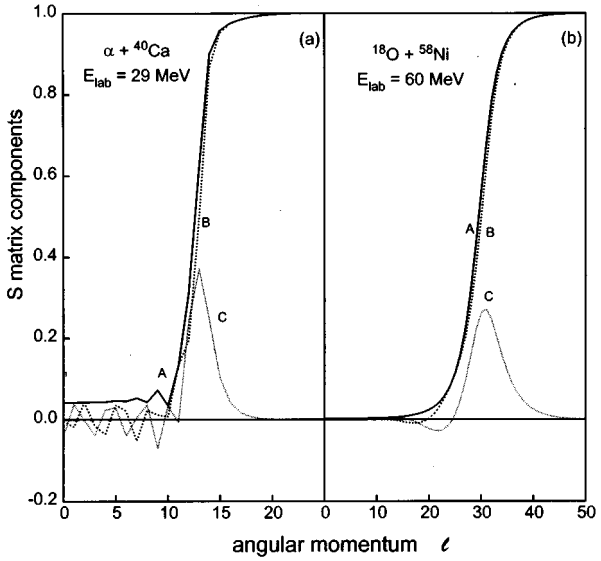

FIG. 2. (a) Plot of ALAS nuclear S matrix with the same potential parameters as that of Fig. 1. (b) Plot of non-ALAS nuclear S matrix [17] with $V_0=90.1$ MeV, $W_0=42.9$ MeV, $r_R=1.22$ fm, $r_I=1.22$ fm, $a_R=0.5$ fm, $a_I=0.5$ fm, $r_C=1.25$ fm. Curves A, B, and C correspond to η_l, $\mathrm{Re}S_l$, and $\mathrm{Im}S_l$, respectively.

mass energy $E_{\mathrm{c.m.}}$, the inner turning point lies quite inside the interior in r space. Due to these features, the reflection function η_l turns out to be highly absorptive for $l<l_g$ and rises rapidly to $\eta_l\simeq 1$ for $l>l_g$.

In Fig. 2, we show the variation of $\mathrm{Re}S_l$, $\mathrm{Im}S_l$, and $\eta_l=|S_l|$ of the nuclear S matrix S_l as a function of l for the $\alpha+{}^{40}\mathrm{Ca}$ system at $E_{\mathrm{lab}}=29$ MeV using the potential given by Eq. (1.1) with the best fit parameters of Ref. [4]. A similar feature of the nuclear S matrix is found at other ALAS energies. One observes the following features: (i) sharp rise of η_l around the grazing partial wave $l_g=13$, (ii) oscillatory structure of $\mathrm{Re}S_l$ and $\mathrm{Im}S_l$ for smaller partial waves in the absorption region $l<l_g$, and (iii) prominent peak of $\mathrm{Im}S_l$ around the grazing partial wave. The oscillatory structure of S_l for lower partial waves can be attributed to the comparatively reduced imaginary part of the optical potential in the surface region. This can be contrasted with a typical non-ALAS heavy ion scattering case ($^{18}\mathrm{O}+{}^{58}\mathrm{Ni}$) in the same figure where the interior partial waves have negligible oscillations with the corresponding η_l approximately zero [17].

The special role of the surface partial waves in ALAS can further be illustrated by studying the classical deflection function $\Theta(l)$ for the real effective potential as defined in Ref. [18] with the scattering angle θ defined as $\Theta=\pm\theta-2m\pi$, $m=0,1,2\cdots$. We have found that for the potential defined by Eq. (1.1) with $\nu=5$, θ tends more towards back angles around $l_g=13$ than for $\nu=1$. This shows that it is the special feature of the effective potential which makes it possible for the scattering to get enhanced at back angles.

We have also searched for resonance poles associated with the few surface waves in the barrier region. In Table I we list the poles in the complex E plane for those partial waves around l_g obtained using the potential parameters from the references listed therein. We see that those partial waves are capable of giving rise to resonance states [19,20].

TABLE I. Poles of the S matrix for α-nucleus systems.

System	E (MeV)	l_g	l	Location of poles (MeV)	Reference
$\alpha+{}^{40}\mathrm{Ca}$	26.45	13	13	$26.47-3.84i$	[4]
$\alpha+{}^{40}\mathrm{Ca}$	26.45	13	14	$31.78-5.51i$	[4]
$\alpha+{}^{16}\mathrm{O}$	25.76	10	10	$23.17-3.66i$	[5]
$\alpha+{}^{16}\mathrm{O}$	25.76	10	11	$31.23-5.45i$	[5]
$\alpha+{}^{26}\mathrm{Mg}$	19.24	10	11	$17.40-3.67i$	[6]
$\alpha+{}^{26}\mathrm{Mg}$	19.24	10	12	$22.87-2.82i$	[6]

However, in the present set of calculations the magnitudes of the imaginary part of the poles are rather large and hence these will give rise to broad resonances which may be difficult to observe experimentally. In the non-ALAS heavy ion system $^{18}\mathrm{O}+{}^{58}\mathrm{Ni}$ [17], we did not find resonance-like poles in the E plane for l around l_g.

In the interior region $l<l_g$, the reflection function η_l oscillates with small amplitude and large frequency whereas in the non-ALAS cases it oscillates rather slowly as shown in Fig. 2. $\mathrm{Im}S_l$ shows sharp prominent peak around l_g in contrast with the non-ALAS case. These imply that it is important to study separately the role of the amplitudes generated by surface partial waves $l\simeq l_g$, outer partial waves $l>l_g+\Delta/2$, and interior partial waves $l<l_g-\Delta/2$ [15]. It is desirable to use the full expansion for the scattering amplitude without isolating the Coulomb amplitude $f_C(\theta)$ because strictly speaking, smaller partial waves get affected more by the nuclear charge distribution than the Ze^2/r type potential. We express the total scattering amplitude as [15]

$$A(\theta)=\frac{1}{2ik}\sum_0^\infty (2l+1)e^{2i\sigma_l}\overline{S_l}P_l(\cos\theta),\quad 0<\theta\leqslant\pi \tag{3.1}$$

as

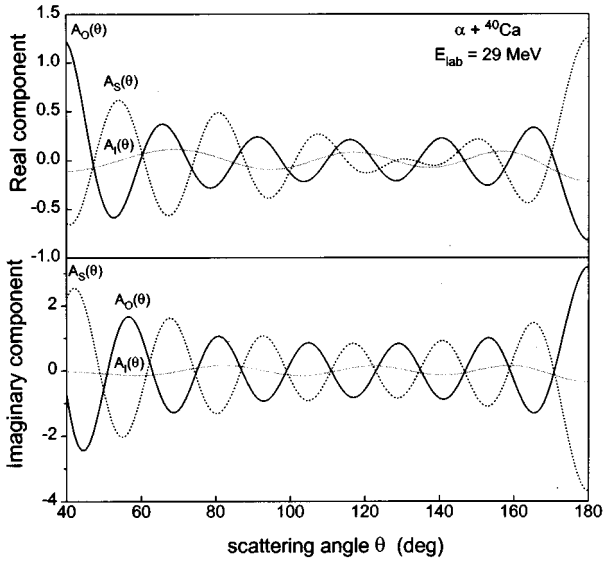

FIG. 3. Real and imaginary parts of the scattering amplitude components with the same potential parameters as that of Fig. 1.

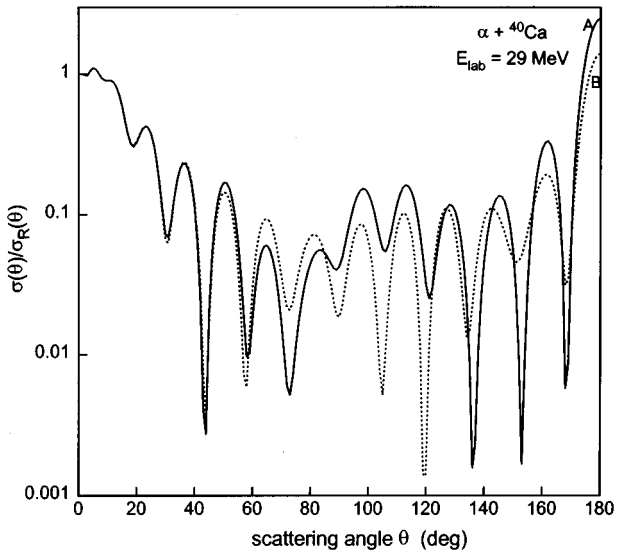

FIG. 4. Effect of neglecting the $A_I(\theta)$ term in the cross section in Eq. (3.2). Curve A corresponds to the actual cross section and curve B to that obtained by ignoring $A_I(\theta)$. The potential parameters are same as that of Fig. 1.

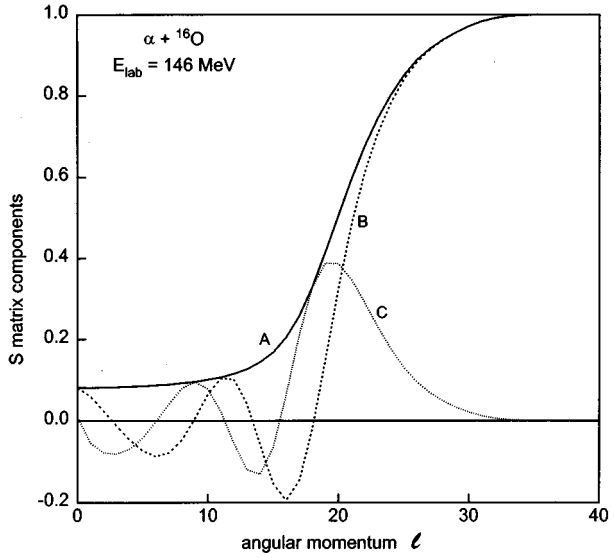

FIG. 5. Nuclear S matrix for non-ALAS case from Ref. [5]. Curves A, B, and C correspond to η_l, $\mathrm{Re}\overline{S_l}$, and $\mathrm{Im}\overline{S_l}$, respectively. The potential parameters are $V_0=38$ MeV, $\alpha=2.174$, $\rho=4.5$ fm, $R_R=4.3$ fm, $a_R=0.6$ fm, $W_0=25$ MeV, $R_I=4.65$ fm, $a_I=0.65$ fm, $r_C=1.3$ fm.

$$A(\theta)=A_I(\theta)+A_S(\theta)+A_O(\theta), \tag{3.2}$$

where

$$A_S(\theta)=\frac{1}{2ik}\sum_{l_i}^{l_f}(2l+1)e^{2i\sigma_l}\overline{S_l}P_l(\cos\theta), \tag{3.3}$$

$$A_I(\theta)=\frac{1}{2ik}\sum_{0}^{l_i-1}(2l+1)e^{2i\sigma_l}\overline{S_l}P_l(\cos\theta), \tag{3.4}$$

$$A_O(\theta)=\frac{1}{2ik}\sum_{l_f+1}^{\infty}(2l+1)e^{2i\sigma_l}\overline{S_l}P_l(\cos\theta)$$

$$\simeq f_C(\theta)-\frac{1}{2ik}\sum_{0}^{l_f}(2l+1)e^{2i\sigma_l}P_l(\cos\theta), \tag{3.5}$$

since $\overline{S_l}\simeq 1$ in this range. Here σ_l is the Coulomb phase shift, l_i and l_f are the partial waves where $\eta_l\simeq 0.1$ and $\eta_l\simeq 0.9$, respectively. Clearly the partial waves $l_i<l<l_f$ are around the grazing partial wave. For the $\alpha+{}^{40}\mathrm{Ca}$ system at $E_{\mathrm{lab}}=29$ MeV, $l_i=11$, $l_f=14$, and $l_g=13$. In the ALAS cases, l_f-l_i is small [15] and for $l>l_f$, the contributions to the amplitude are primarily Coulombic. Similarly, for $l<l_i$, the contribution from any given partial wave can be expected to be small and because of oscillations in $\overline{S_l}$, cancellations may occur further reducing the relative importance of $A_I(\theta)$. In Fig. 3, we show the real and imaginary parts of $A_I(\theta)$, $A_S(\theta)$, and $A_O(\theta)$ for the scattering of $\alpha+{}^{40}\mathrm{Ca}$ at $E_{\mathrm{lab}}=29$ MeV. In Fig. 4 we plot $\sigma(\theta)$ and $|A_S(\theta)+A_O(\theta)|^2$, i.e., the cross section obtained by ignoring the contribution of the interior term $A_I(\theta)$. We see that ignoring $A_I(\theta)$ in the cross section causes only marginal changes in the structure of $\sigma(\theta)$ and that the rise of $\sigma(\theta)$ at back angles is primarily a surface phenomenon governed by the interference between $A_S(\theta)$ and $A_O(\theta)$. Even in the case of ${}^{16}\mathrm{O}+{}^{28}\mathrm{Si}$, $A_I(\theta)$ is comparatively small [15]. The conclusion is that the ALAS can be attributed primarily to the interference between the surface and predominantly Coulombic outer partial waves.

Using the potential of Michel *et al.* [5], we take a close look at $\alpha+{}^{16}\mathrm{O}$ scattering at 146 MeV where ALAS vanishes. This potential has the form

$$V(r)=-V_0\frac{1+\alpha\,\exp[-(r/\rho)^2]}{\{1+\exp[(r-R_R)/2a_R]\}^2}$$

$$-i\frac{W_0}{\{1+\exp[(r-R_I)/2a_I]\}^2}+V_C(r). \tag{3.6}$$

In Fig. 5 we show the reflection function η_l, $\mathrm{Re}\overline{S_l}$, and $\mathrm{Im}\overline{S_l}$ for this potential with best fit parameters from Ref. [5]. We see that the band in l space through which η_l rises from 0.1 to 0.9 is quite large having around 18 partial waves. This defines a wide surface of width $\Delta r\simeq 1.9$ fm in contrast with the ALAS case at $E_{\mathrm{lab}}=32$ MeV for the same potential where $\Delta r\simeq 1$ fm, $l_i=9$, and $l_f=11$. Thus in the non-ALAS case, the partially absorptive α-nucleus S_l are spread over a wide region in the l space. Further η_l for small l is also comparatively larger. In such cases there is large cancellation of contributions from different partial waves leading to highly suppressed oscillations at large angles.

It is clear from the above results that the sum of surface and outer region partial waves can generate ALAS with $A_I(\theta)$ contributing marginally. When $A_S(\theta)$ consists of a very small number of partial waves around l_g, both $A_S(\theta)$ and $A_O(\theta)$ are dominated by similar Legendre polynomial-like terms with different amplitudes. This is elaborated mathematically in Ref. [15]. The same situation does not arise in non-ALAS cases because of smoother variation of η_l and comparatively larger and less oscillatory behaviour of S_l for

smaller l as can be seen by comparing Fig. 5 and Fig. 2. Hence we conclude that within the frame work of fully quantum-mechanical l space analysis, it is the interference of partial waves from the narrow l window around l_g and the predominantly Coulombic outer partial waves which gives rise to enhanced back angle oscillations. The phenomenological optical potentials such as the one used in Refs. [4–6] to generate ALAS implicitly simulate the desired features in the S matrix.

The interpretation of ALAS given by Brink and Takigawa [14] is a semiclassical approach using the WKB method. Here, the nuclear S matrix is split up into a barrier component $S_B(l)$ and an internal component $S_I(l)$ corresponding to waves reflected at the outer turning point of the barrier and inner turning point of the centrifugal barrier. This division of the S matrix is in the r space. However, the Coulomb amplitude is separated and treated as a full entity without r space splitting. For normal heavy ion systems with strong absorption the internal wave is highly damped but for potentials with weak absorption, these two terms interfere giving rise to the enhancement of $\sigma(\theta)$ at back angles. Thus in this picture, ALAS occurs primarily due to the interference between diffracted waves (interior) and refracted waves (barrier).

In conclusion, we find that at energies where ALAS occurs in α-nucleus systems, $\mathrm{Re}V_{\mathrm{eff}}(r)$ is remarkably flat for partial waves close to l_g and $\mathrm{Im}V_{\mathrm{eff}}(r)$ is small around the barrier region. Also $\mathrm{Im}S_l$ peaks sharply around l_g with oscillatory structure for $l<l_g$. η_l also rises sharply around l_g. The nuclear S matrix around $l=l_g$ is found to have resonance-like poles for potentials generating ALAS. Splitting $A(\theta)$ into three terms $A_I(\theta)$, $A_S(\theta)$, and $A_O(\theta)$ corresponding to interior, surface, and outer terms, we find that ALAS can be primarily attributed to the interference between $A_S(\theta)$ and $A_O(\theta)$.

[1] U. Atzrott, P. Mohr, H. Abele, C. Hillenmayer, and G. Staudt, Phys. Rev. C **53**, 1336 (1996).

[2] Th. Delbar, Gh. Gregoire, G. Paic, R. Ceuleneer, F. Michel, R. Vanderporten, A. Budzanowski, H. Dabrowski, L. Freindl, K. Grotowski, S. Micek, R. Planeta, A. Strzalkowski, and K. A. Eberhard, Phys. Rev. C **18**, 1237 (1978).

[3] V. Avrigeanu, P. E. Hodgson, and M. Avrigeanu, Phys. Rev. C **49**, 2136 (1994).

[4] H. P. Gubler, U. Kiebele, H. O. Mayer, G. R. Plattner, and I. Sick, Nucl. Phys. **A351**, 29 (1981).

[5] F. Michel, J. Albinski, B. Belery, Th. Delbar, Gh. Gregoire, B. Tasiaux, and G. Reidemeister, Phys. Rev. C **28**, 1904 (1983).

[6] J. Lega and P. C. Macq, Nucl. Phys. **A218**, 429 (1974).

[7] P. Braun-Munzinger, G. M. Berkowitz, T. M. Cormier, C. M. Jachcinski, J. W. Harris, J. Barrette, and M. J. LeVine, Phys. Rev. Lett. **38**, 944 (1977).

[8] S. Y. Lee, Nucl. Phys. **A311**, 518 (1978).

[9] P. Braun-Munzinger and J. Barrette, Phys. Rep. **87**, 209 (1982).

[10] A. M. Kobos, B. A. Brown, R. Lindsay, and R. Satchler, Nucl. Phys. **A425**, 205 (1984).

[11] W. E. Frahn, Nucl. Phys. **A337**, 324 (1980).

[12] W. E. Frahn, M. S. Hussein, L. F. Canto, and R. Donangelo, Nucl. Phys. **A396**, 166 (1981).

[13] W. E. Frahn and K. E. Rehm, Phys. Rep. **37C**, 1 (1975).

[14] D. M. Brink and N. Takigawa, Nucl. Phys. **A279**, 159 (1977).

[15] C. S. Shastry and I. Parija, Phys. Rev. C **27**, 2042 (1983).

[16] I. Parija, R. K. Satpathy, and C. S. Shastry, Phys. Rev. C **29**, 1552 (1984).

[17] R. Videback, P. R. Christensen, O. Hansen, and K. Ulbak, Nucl. Phys. **A256**, 30 (1976).

[18] D. M. Brink, *Semi-Classical Methods for Nucleus-Nucleus Scattering* (Cambridge University Press, Cambridge, 1985), p. 38.

[19] B. Sahu, B. M. Jyrwa, P. Susan, and C. S. Shastry, Phys. Rev. C **44**, 2729 (1991).

[20] P. Susan, B. Sahu, B. M. Jyrwa, and C. S. Shastry, J. Phys. G **20**, 1234 (1994).